VI International Conference on Computational Methods in Marine Engineering
MARINE 2015
F. Salvatore, R. Broglia and R. Muscari (Eds)

MARINE APPLICATION OF FLETTNER ROTORS: NUMERICAL STUDY ON A SYSTEMATIC VARIATION OF GEOMETRIC FACTOR BY DOE APPROACH

A. DE MARCO*, S. MANCINI*, C. PENSA*, R. SCOGNAMIGLIO*, L. VITIELLO*

* Università degli Studi di Napoli "Federico II", Italy
Email: agostino.demarco@unina.it, simone.mancini@unina.it, claudio.pensa@unina.it, raffaele.scognamiglio@unina.it, luigi.vitiello@unina.it - Web page: http://www.dii.unina.it

Key words: Computational Fluid Dynamics, Marine Engineering, Statistical Analysis, Design of Experiment, Flettner Rotors

Abstract. Flettner Rotors (*FR)* are spinning cylinders, which produce fluid dynamic lift by using the Magnus Effect. The Magnus force can be much greater in magnitude than the wing lifting force, given the same projected area and dynamic air pressure. The *FR* was used for ship's propulsion system in the 1920's. Nowadays, the *FR* is being seriously examined due to the necessity of renewable resources use.
Since several months, the *Dipartimento di Ingegneria Industriale* of the *Università degli Studi di Napoli "Federico II"* has started a research about preliminary analysis for marine application of *FR* through Unsteady Reynolds Average Navier Stokes (*U-RANS*) simulations for 3D flow past a full-scale rotating [1].
The aerodynamic forces, Lift (*L*), Drag (*D*) and Aerodynamic Efficiency (*L/D*) of a *FR* are the response variables and are influenced by the following control factors:

- Spin Ratio (*SR*), *i.e.* the ratio of circumferential-cylinder-velocity-to-free stream-velocity;
- Aspect Ratio (*AR*), *i.e.* the ratio between the cylinder length and diameter;
- Endplate Ratio (De/D_0), *i.e.* ratio between the endplates diameter and cylinder diameter;

In this work, a preliminary assessment of numerical setup has been conducted by comparison with experimental investigation carried out by Badalamenti and Prince at *City University of London* and published in [2], [3]. The tested cylinder has $AR = 5.1$, $D_0 = 0.0889$ m, $De/D_0 = 2$.
A statistical approach based on Design of Experiment (*DoE*) has been applied to the testing program of *FR* in order to evaluate the functional relationship and the interaction between the control factors *SR*, *AR* and De/D_0 which influence the response variables *L*, *D* and *L/D*.
All tests are developed through *U-RANS* simulations for *3D* flow past rotating cylinder. The *U-RANS* simulations have been performed by using the commercially available flow simulation software *CD-Adapco STAR CCM+ v. 9.06.009.*

1 INTRODUCTION

Flettner Rotors are spinning cylinders, which produce fluid dynamic lift by using the Magnus Effect. The Magnus force can be much greater in magnitude than the wing lifting force, given the same projected area and dynamic air pressure. Anton Flettner, a German Aviation Engineer, used spinning cylinders for the first time as a ship's propulsion system in the 1920's. Further commercial development did not take place before the 21st Century, when the growing sensibility to the necessity of an anti-pulling policy has revalued the *FR* potentialities. In Figure 1, the E-Ship 1, launched by Enercon Wind Energy Company in 2010, and the Finnish *Ro-Ro* cargo ship Estraden (modified by Norsepower Company in 2014) are shown.

Figure 1 E-Ship 1 (Enercon Wind Company) and Estraden *Ro-Ro* cargo (Norsepower Company)

In this paper, a statistical Design of Experiment (*DoE*) has been applied to investigate lift, drag and aerodynamic efficiency of *FR*. *DoE* is a statistical methodology for a systematically approach used for problems with a large number of variables. Moreover, *DoE* approach is able to predict, economically, accurately and in few experimental runs, the responses of the system by approximate mathematical models. This approach is similar to that reported in [4] and [5], wich represent two recent applications of this method in marine engineering field.

2 PRE-EXPERIMENTAL PLANNING

A pre-design sheet has been implemented by following the systematic approach to planning a design experiment proposed in [6].
The main sheets contain information about the objective of the experimentation, the relevant background, the response variables and the factors (i.e., control, held-constant and nuisance factors).
In this first experimental phase, the objective was to characterize the response variable *L* and *D* forces produced by *FR* which depend on various parameters. The characteristics of a rotating body in cross-flow and as well as the most important parameters are briefly summarized below. The relevant background has been derived from a previous work [1].
The study of the factors involved in the experimentation is a crucial task. In fact, during the first step was established a list of all factors which influence the experimentation, whereas during the second step has been classified each factor as a control, held-constant or nuisance factor [6].

2.1 Control factors

The control factors adopted in this work are:

- Spin Ratio (*SR*).
- Aspect Ratio (*AR*).
- End Plate Geometry (De/D_0).

Factors *SR*, *AR* and De/D_0 are quantitative parameters. The effects of these parameters on the underpinning physics of the *FR* are described in the following.

2.1.1 Spin ratio

SR is the ratio of circumferential-cylinder-velocity-to-free stream-velocity and the levels assumed for this factor are 1 or 2. The general trend of the C_L and C_D curves is growing with *SR* value, except for cylinders without *EP* working at the highest *Re* values and for the C_D given by Thom [7] whose trend is probably due to the very high *AR*.
The flow phenomenology around a circular cylinder, is rather complex and consists of tip vortices and alternate vortex shedding between the rotor ends. The vortex shedding occurs $Re < 8.0 \cdot 10^6$ [8]. The Strouhal numbers, defined by $S_t = f D_0/U$, describe the oscillating flow past a rotating cylinder where f is the frequency of vortex shedding and U is the free-stream velocity. Low Strouhal number ($S_t < 1.0 \cdot 10^4$) indicates a quasi-steady flow. The Kàrman vortex street occurs for $SR = 0.0 \div 2.0$. The eddies are formed and shed alternately on two sides of the cylinder. The long eddy formation occurs for $SR = 0.0$ and is considerably shortened for higher *SR*. Vortex formation and shedding does not occur for $SR > 2.0$, whereas for $SR = 3.0$, a quasi-steady-state is observable. In [3] a deep analysis on vortex shedding is explained.
In this paper, *SR* variations have been obtained by only changing the free-stream-velocity (constant circumferential-cylinder-velocity)

2.1.2 Aspect ratio

AR is the ratio between the cylinder length and diameter and the levels assumed for this factor are 2, 4 and 6. The effect of *AR* on wings is similar to rotors. Swanson [9] concluded in his review paper that a general trend is indicated by experimental data due to the aspect ratio of rotors: the smaller the aspect ratio the smaller the maximum lift obtained and the smaller the velocity ratio at which this maximum is reached. Leakage flow and consequent pressure equalization around the ends of the cylinder is responsible for this effect. In Swanson [9] it is demonstrated also that, for very high *AR* values, lift can reach values higher that the maximum theoretical limit predicted in [10].

2.1.3 Tip geometry

The idea of applying endplate to the rotors was suggested in [10]. Ten years later, Thom in [7] investigated the effect of large *EP* with $De/D_0 = 3.0$. In this paper the level assumed for this factor are 1, 2 and 3. The studies suggest that the *EP* substantially causes the doubling of the lift at high velocity ratios $SR = 2.0$. In [2], it is shown that for a cylinder with $AR = 5.1$ and

diameter ratios ranging from De/D_0 = 1.1 to 3.0, the effects of the increases of De/D_0 and *AR* are similar: a growing trend of lift and a delay of the occurrence of its maximum for higher *SR*. The choice of *EP* size for the best performance was found to be dependent on *SR*. At low spin ratio, *SR* = 1.0, smaller plates generally give lightly smaller drag. For applications at moderate spin ratio, 1.0 < *SR* < 3.0, larger plates are preferred, so as to delay the increase in induced drag. For high spin ratio applications, *SR* > 3, smaller plates are preferred in such a way drag quickly approaches a limit, as it is remarkable in Figure 2 a and b.

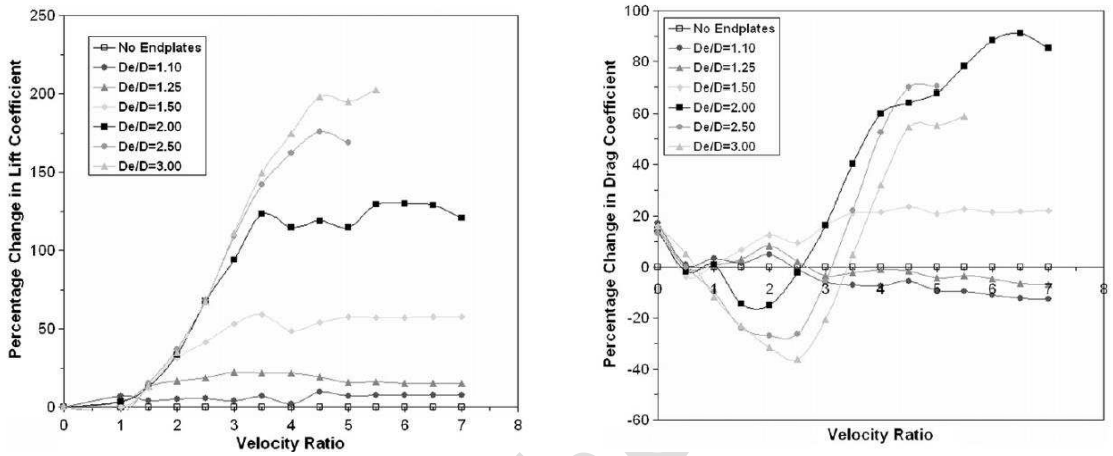

(a) (b)

Figure 2 Effect of De/D_0 on Lift (a) and Drag (b) Coefficients [8]

2.2 Held Constant and nuisance factors

Held-constant factors are controllable factors whose effects are not of interest in this experimental phase. In this experimentation, the surface roughness has been considered as held-constant factors and no surface roughness has been applied. Advantages and disadvantages of applying a rough surface to a *FR* are exhaustively reported in [8].
Nuisance factors are uncontrolled factors, which cannot be controlled from a technological or economical point of view. There are some potential nuisance factors which could influence the *CFD* experiments. In this case, the *Re* has been considered the main nuisance factor. In fact the variation of *Re* is due to the variation of free-stream-velocity.
The *Re* has a significant influence on the lift magnitude of rotating cylinder at *SR* < 1.0 (with *Re* based on the cylinder diameter) in terms of lift variation [9]. The effect is particularly pronounced when $Re > 6 \cdot 10^6$. A similar has been effect was seen in the drag data.

3 EXPERIMENTAL DESIGN AND SET-UP

In the pre-experimental phase, three factors have been considered important and a mixed-level full factorial $3^2 \times 2^1$ design has been adopted. Table 1 summarizes the levels of control factors and their settings. Table 2 shows the $3^2 \times 2^1$ design matrix and corresponding response variable, giving a total of 18 experimental runs.

JMP® Pro 11.2.0 from *SAS* institute software has been adopted to design the experiment and analyse the results.

Table 1 Control factors

Control factors	Symbol	Low value	Mid value	High value
Spin Ratio	*SR*	1	-	2
Aspect Ratio	*AR*	2	4	6
Tip Geometry	De/D_0	1	2	3

The tests have been reproduced numerically by *U-RANS* simulation software *CD-Adapco STAR-CCM+ v. 9.06*.

Table 2 Matrix for the $3^2 \times 2^1$ design

Std order	Pattern	*SR*	*AR*	De/D_0	*L [N]*	*D [N]*	*L/D*
1	11	2	2	1	0.00038	0.00042	0.90821
2	21	2	4	1	0.00159	0.00100	1.59562
3	22	2	4	2	0.00251	0.00085	2.96698
4	−32	1	6	2	0.00512	0.00257	1.99081
5	33	2	6	3	0.00383	0.00078	4.91937
6	−31	1	6	1	0.00363	0.00178	2.03392
7	13	2	2	3	0.00125	0.00035	3.59648
8	−12	1	2	2	0.00147	0.00079	1.85061
9	−13	1	2	3	0.00172	0.00101	1.71025
10	32	2	6	2	0.00381	0.00104	3.65503
11	−33	1	6	3	0.00565	0.00279	2.02785
12	12	2	2	2	0.00122	0.00057	2.13001
13	31	2	6	1	0.00517	0.00311	1.66329
14	−21	1	4	1	0.00270	0.00157	1.71576
15	23	2	4	3	0.00256	0.00061	4.18440
16	−11	1	2	1	0.00098	0.00076	1.29289
17	−22	1	4	2	0.00346	0.00261	1.32715
18	−23	1	4	3	0.00381	0.00299	1.27407

3.1 ASSESSMENT OF THE CFD PREDICTION

In the following, the numerical setup is presented and the comparison with experimental data for a cylinder configuration with end plates of diameter $De = 2D_0$ and $AR = 5.1$ (Figure 3) given by Badalamenti and Prince [2], [3] is discussed.

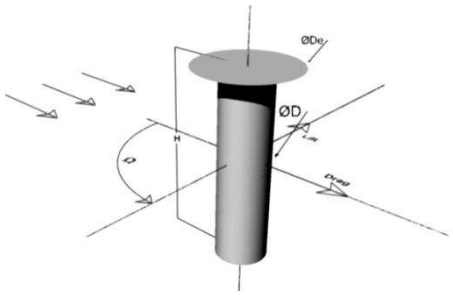

Figure 3 Main geometry parameters

3.1.1 Numerical setup

In all the simulations, a full second order discretization of the convective term has been used. For the temporal discretization a second order backward Euler scheme has been used. All the calculations have been performed incompressible. Fully turbulent calculations have been carried out by using the *k-ω* Shear-Stress-Transport (*SST*) turbulence model. The time step chosen is 1.25 10^{-3} s, according with previous work [1]. All mesh tested are polyhedral unstructured grid (Figure 4 b).

3.1.2 Boundary conditions

In order to reduce the computational effort, only half of the cylinder has been modelled and a symmetry plane has been used at the mid-length. A velocity inlet boundary condition has been set on the front part of the domain with a prescribed velocity. On the rear part of the domain, a pressure outlet boundary condition has been imposed with a relative pressure of 0.0 Pa. On the opposite side of the domain, a symmetry boundary condition has been also used. Around the rotor a cylindrical area of overlap between the rotating mesh and fix domain has been, since this is a necessary condition for using the overset mesh methodology (Figure 4 a).

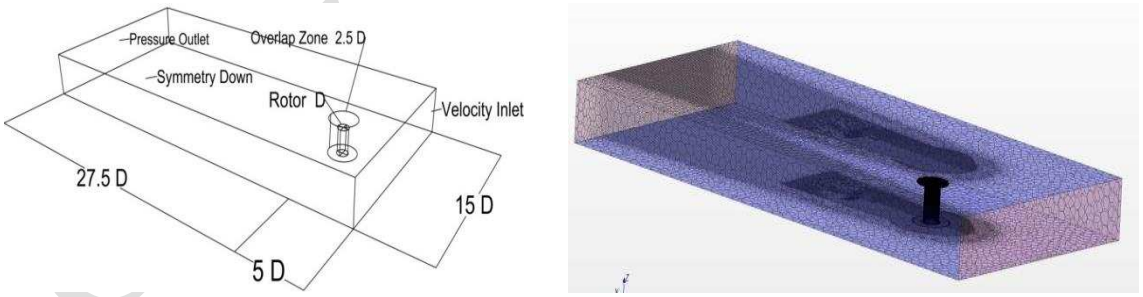

Figure 4 Simulation domain with boundary conditions (a) and mesh visualization (b)

3.1.3 Grid-dependence study

Grid uncertainty is evaluated according to Grid Convergence Index (*GCI)* method derived by Roache [11]. Three grid have been used (case A – Coarse grid, case B – Medium Grid, case C

– Fine Grid) with refinement factor (r) equal to $\sqrt{2}$. The generalized Richardson Extrapolation (*RE*) has been used to estimate the grid error $\delta^*_{RE_{G,1}}$ (convergence condition as shown in Figure 5) with p_i order of accuracy. Then, the grid uncertainty has been evaluated by the following expression:

$$U_G = F_S \cdot \left|\delta^*_{RE_{G,1}}\right|,\ \delta^*_{RE_{G,1}} = \frac{\varepsilon_{G,21}}{r_G^{\,p_G} - 1},\ p_i = \frac{\ln(\varepsilon_{G,32}/\varepsilon_{G,21})}{\ln(r_G)} \tag{1}$$

where F_S is a safety factor that has been assumed equal to *1.25* (for three grid case) [11] and $\varepsilon_{G,kj}$ equal to the changes between the coarser grid solution and finer grid. The iterative convergence for each sub–step, has been found negligible with respect to the grid uncertainty.

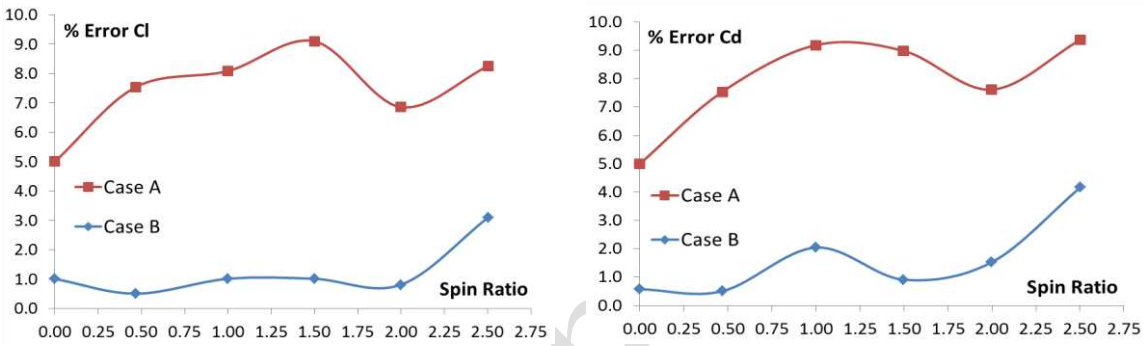

Figure 5 C_l and C_d percentual error of finer grid (Case C)

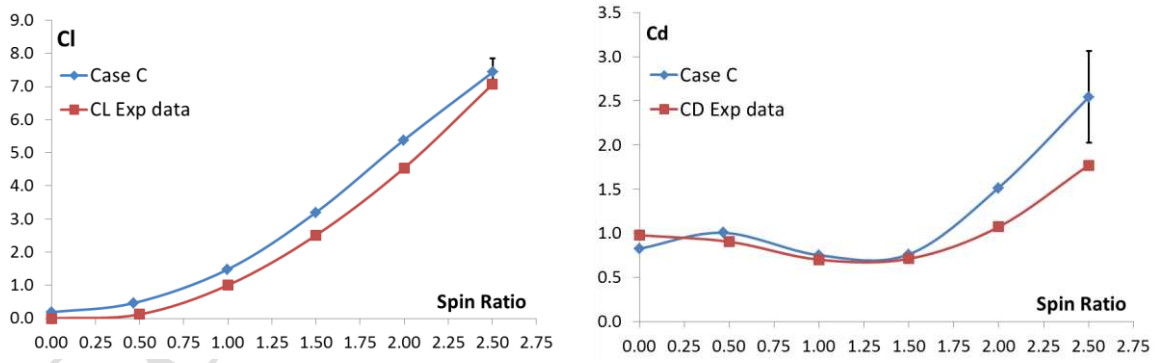

Figure 6 Comparison between experimental data and numerical results with grid uncertainty

3.1.4 Comparison with experimental data

The numerical results obtained with grid case C have been compared with the experimental data as shown in Figure 6. The C case has been chosen since it guarantees an accurate solution without an excessive effort than case B (2100 s *CPU* time for timestep instead 1900 s *CPU* time for timestep to obtain a convergent solution).

4 RESULTS AND DISCUSSION

With reference to variables reported in Table 1, the following multiple linear regression models, proposed for *L*, *D* and *L/D*, are shown:

$$L = \beta_0 + \beta_1\left(\frac{Sr-1.5}{0.5}\right) + \beta_2 Ar + \beta_3\frac{D_e}{D} + Z \quad (2)$$

$$D = \beta_0 + \beta_1\left(\frac{Sr-1.5}{0.5}\right) + \beta_2 Ar + \beta_3\frac{D_e}{D} + \beta_4\left(\frac{Sr-1.5}{0.5}\right)\left(\frac{D_e}{D}-2\right) + Z \quad (3)$$

$$L/D = \beta_0 + \beta_1\left(\frac{S_r-1.5}{0.5}\right) + \beta_2 A_r + \beta_3\frac{D_e}{D} + \beta_{12}\left[\left(\frac{S_r-1.5}{0.5}\right)(A_r-4)\right] + \beta_{13}\left[\left(\frac{S_r-1.5}{0.5}\right)\left(\frac{D_e}{D}-2\right)\right] + Z \quad (4)$$

where *Z* has been assumed to be a normal random error component with mean equal to zero and unknown variance σ^2. Trivially note that in the equations (2), (3) and (4) as in any regression model, the dimensional homogeneity is ensured by the regression coefficients *βij* reported in equations (2), (3) and (4) and in Table 3.

The Analysis of Variance (*ANOVA)* method (with α = 0.05) has been applied to test the statistical significance of the control factors, the main effects and the two-factor interactions. The regressor variable and their interaction have been chosen based on *ANOVA* method, and a diagnostic checking has been successfully performed via graphical analysis and normality test of residuals. Moreover, *Actual by predicted* plots, reported in Figure 7 a, b and c, show the adequacy of the fit of the regression model and they allow to check the validity of the underlying assumptions.

Therefore, the usefulness of this model must be investigated through goodness-of-fit indices R^2, R^2 adjusted (R^2_{adj}), standard deviation of residuals *(S)* − and through prediction indicators − Predicted REsidual Sum of Squares *(PRESS)*, which are well-known to the statistical literature [12], [13].

In Table 3 there are the main results of the *L*, *D* and *L/D* regression analysis based on data shows in design matrix (Table 2). In Figure 8 a, b and c, the prediction profiler of response variable *L*, *D* and *L/D* as function of control factors *SR*, *AR* and De/D_0 are shown.

Table 3 Regression Analysis Coefficients: *L* (left), *D* (right) and *L/D* (down)

$\hat{\beta}_0$	$\hat{\beta}_1$	$\hat{\beta}_2$	$\hat{\beta}_3$
-1.27E-03	3.46E-04	9.48E-03	4.09E-3

S	R^2	R^2_{adj}	*PRESS*
5.51E-04	89.88	87.72	7.77E-06

$\hat{\beta}_0$	$\hat{\beta}_1$	$\hat{\beta}_2$	$\hat{\beta}_3$	$\hat{\beta}_{13}$
7.88E-05	4.52E-04	3.40E-04	9.17E-06	-4.56E-04

RMSE	R^2	R^2_{adj}	*PRESS*
5.5E-04	74.92	67.20	8.06E-06

$\hat{\beta}_0$	$\hat{\beta}_1$	$\hat{\beta}_2$	$\hat{\beta}_3$	$\hat{\beta}_{12}$	$\hat{\beta}_{13}$
5.16E-02	5.78E-01	2.00E-01	7.09E-01	1.00E-01	7.14E-01

RMSE	R^2	R^2_{adj}	*PRESS*
2.6E-01	96.14	94.53	8.06E-06

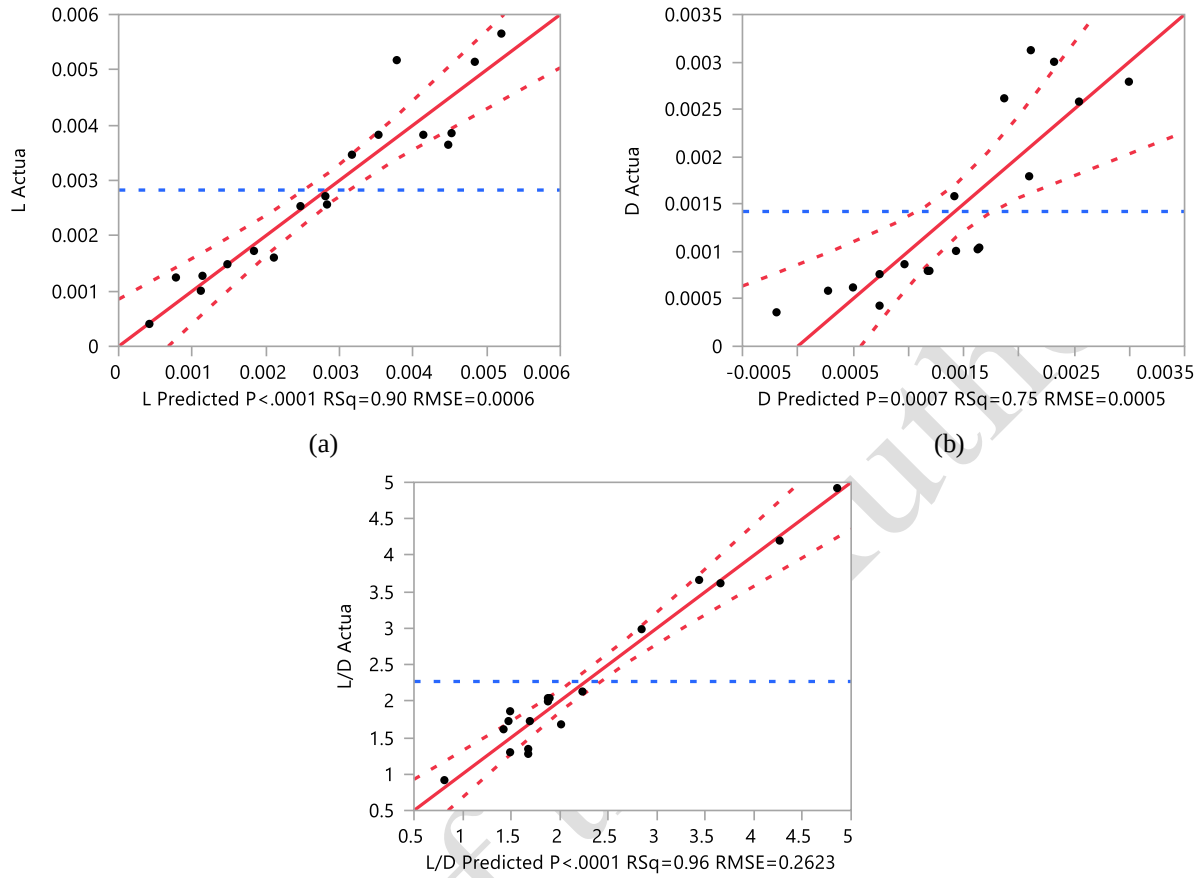

Figure 7 Actual by predicted Plot for: *L* (a), *D* (b) and *L/D* (c)

In Figure 8 a, it is remarkable to note that *L* decreases with growing *SR*, whose variation has been attained reducing free stream velocity. *AR* is the most significant control factor for the *L* generation. In Figure 8 b *D* shows similar behaviours to the trends of the *L*.

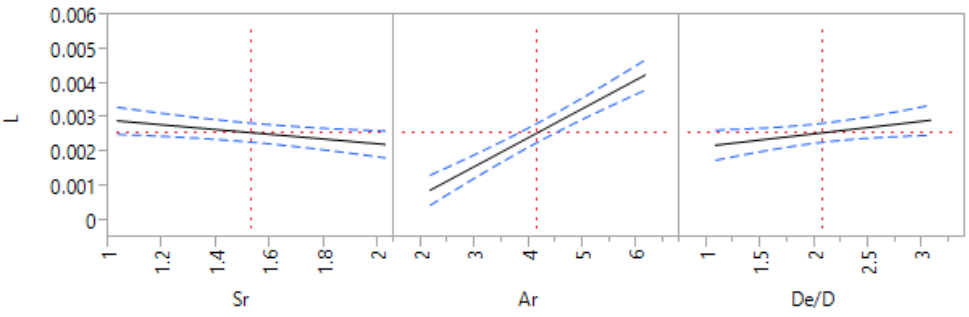

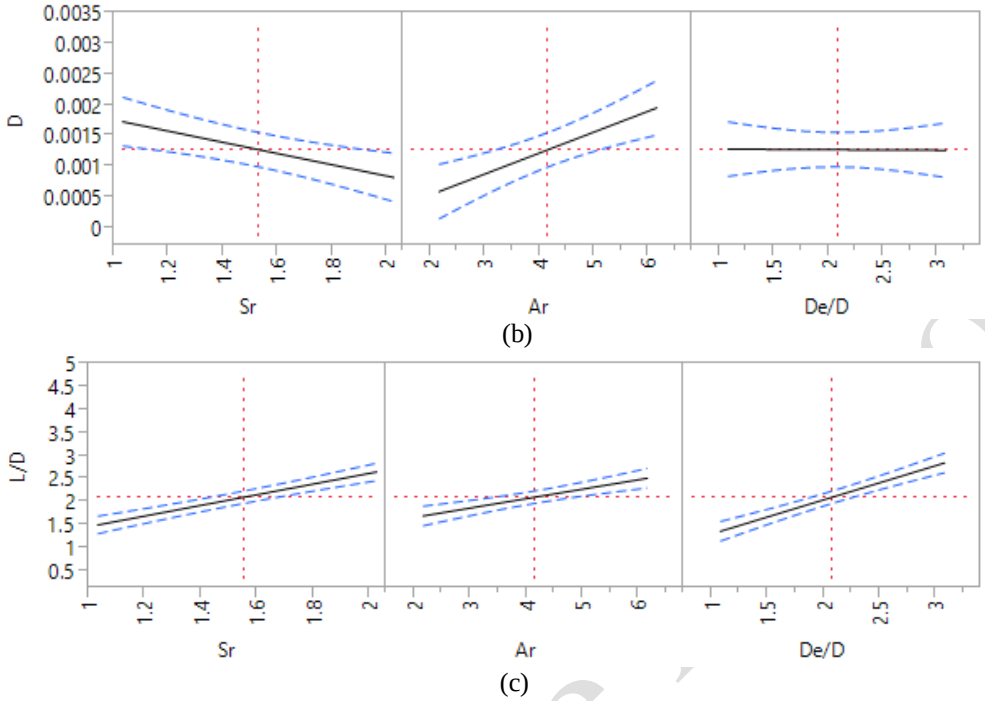

Figure 8 Prediction profiler for: (a) Lift, (b) Drag and (c) *L/D*

Moreover are shown the two-factor interactions profiles, in particular *SR* - De/D_0 for the *D* in Figure 9 and *SR* – *AR*, *SR* - De/D_0 for the aerodynamic efficiency in Figure 10. This is the main contribution offered by *DoE* in the context of this experimentation.
In more detail, in Figure 9, both interactions between De/D_0 - *SR* and *SR* - De/D_0 are antisynergic type and involve the factor *SR* up to then set 1 for the first interaction and the factor De/D_0 down to then set 3.
In Figure 10, the mutual interactions between *SR* - *AR* are synergic type, whereas the mutual interactions between De/D_0 - *SR* are antisynergic type.

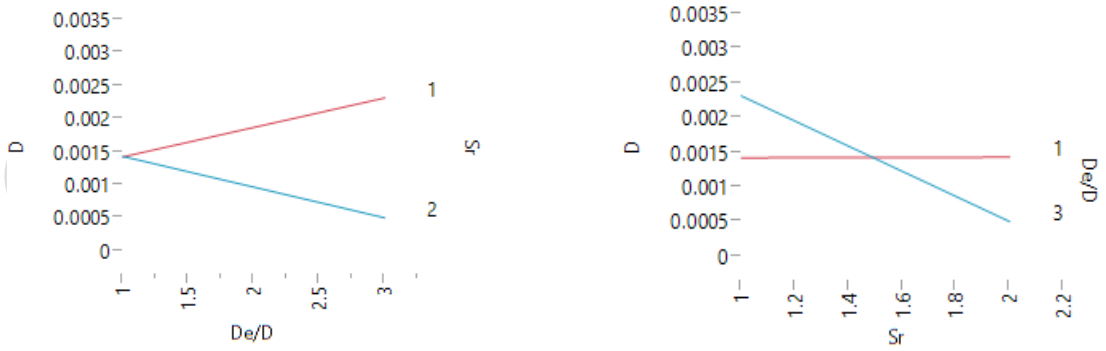

Figure 9 *D* Interaction Profiles

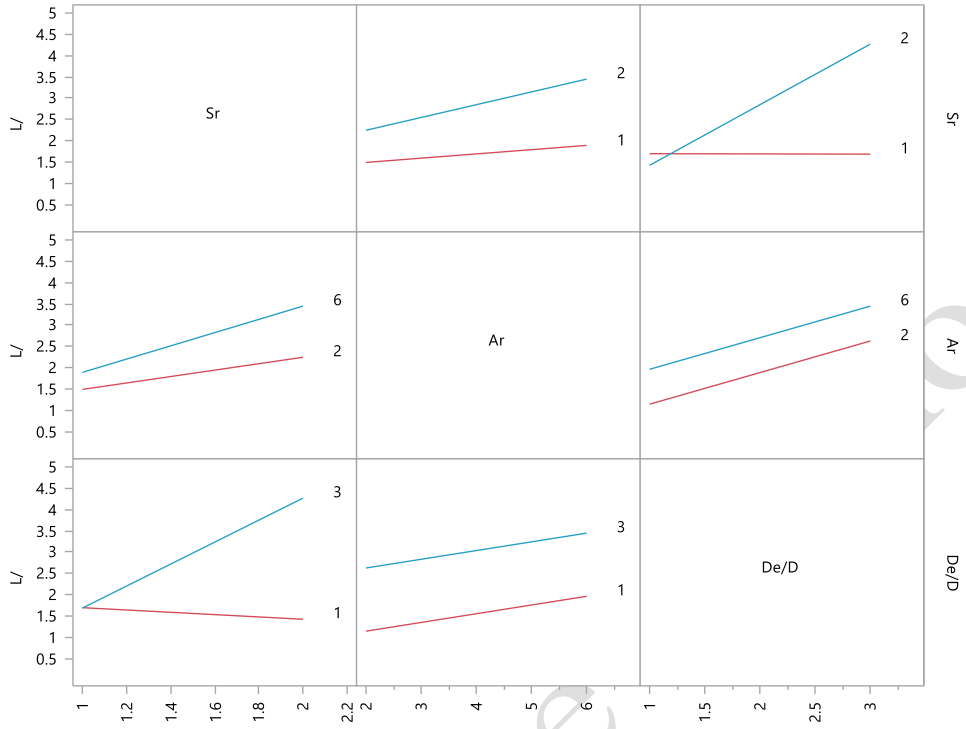

Figure 10 *L/D* Interaction Profiles

5 CONCLUSIONS

In this paper, a systematic approach is proposed to identify the effectiveness and industrial usefulness of *FR*. The main conclusions are summarized in the following.

- The validation of the *CFD* simulations shows errors within 10% for *L* as compared with experimental data (Figure 6). Regarding *D*, the errors are very small up to *SR* = 1.5 and arise dramatically for higher *SR* (Figure 6). These trends seem to be related to the effectiveness limits of turbulence models applied.
- Three regression equations effective to quantify *L*, *D* and aerodynamic efficiency have been proposed (the other one known by the authors does not allow a practical calculation [8], [9]).
- The goodness of fit highlighted by *P-value* and R^2 is better for *L* then for *D*. This is partially due to the higher uncertain of the drag numerical evaluation, that is consistent with a more intrinsically unsteadiness of the drag force.
- With reference to equations (3) and (4), *ANOVA* analysis shows significant interactions between *SR* - De/D_0 for the *D* and *SR* - *AR* and *SR* - De/D_0 for the aerodynamic efficiency. On other hand no interactions have been found for *L*.
- The performance of the interactions identified previously is in line with the physics of the problem, as explained in the Section 2.

6 FUTURE WORKS

In the future, devices will be studied to improve the effectiveness of the *FR* as different form of the *EP* or not rotating *EP*.

7 ACKNOWLEDGMENTS

The authors gratefully acknowledge the availability of the Calculation Centre *SCoPE* of the *Federico II* University and thanks to *SCoPE* academic staff for the given support.

9 REFERENCES

[1] A. De Marco, S. Mancini and C. Pensa, "Preliminary Analysis for Marine Application of Flettner Rotors," in *INT-NAM*, Istanbul, Turkey, 2014.

[2] C. Badalamenti and S. Prince, "Effects of endplates on a rotating cylinder in crossflow," in *AIAA*, Honolulu, Hawaii, 2008.

[3] N. Thouault, N. Breitsamter, J. Seifert, C. Badalamenti and S. A. Prince, "Numerical Analysis of a Rotating Cylinder with Spanwise Discs," in *ICAS*, Nice, France, 2010.

[4] D. Hawkins and L. M. Lye, "Use of DOE methodology for investigating conditions that influenece the tension in marine risers for FPSO ships," in *1st International Structural Speciality Conferrence*, Calgary, Alberta, 2006.

[5] M. F. Islam and L. M. Lye, "Combined use of dimensional analysis and modern experimental design methodologies in hydrodynamics experiments," *Ocean Engineering*, no. 36, pp. 237-247, 2009.

[6] D. E. Coleman and D. Montgomery, "A Systematic Approach to Planning for a Design Industrial Experiment," vol. 35, 1993.

[7] A. Thom, "Effects of discs on the air forces on a rotating cylinder," 1934.

[8] J. Seifert, "A review of the Magnus effect in aeronautics," *Progress in Aerospace Sciences*, pp. 17-45, 2012.

[9] M. W. Swanson, "The Magnus effect: a summary investigations to date," *Journal of basic Enginneering Transactions of ASME*, 1961.

[10] L. Prandtl, "The Magnus effect and wind-powered ships," *Naturwissenschaften*, vol. 13, pp. 1787-1806, 1925.

[11] J. P. Roache, "Code Verification by the Method of Manufactured Solutions," *Journal of Fluids Engineering*, vol. 1, no. 124, pp. 4-10, 2002.

[12] D. Montgomery, G. Runger and N. Hubele, Enginnering Statistic, Wiley & Sons, 2011.

[13] D. Broadhurst, R. Goodacre, A. Joanes, J. J. Rowland and D. B. Kell, "Genetic Algorithms Method for Variable in Multiple Linear Regression and Partial Least Squares, with Application to Pyrolysis mass Spectrometry," *Analytica Chimica Acta*, no. 348, 1997.